## Terahertz Field Control of Electronic-Ferroelectric Anisotropy at Room Temperature in LuFe<sub>2</sub>O<sub>4</sub>

Hirotake Itoh®, 1,\*,† Ryusei Minakami, Hongwu Yu®, Ryohei Tsuruoka, Tatsuya Amano®, Yohei Kawakami®, Shin-ya Koshihara®, Kosuke Fujiwara®, 3,‡ Naoshi Ikeda®, Yoichi Okimoto®, 2,8 and Shinichiro Iwai® 1, Department of Physics, Tohoku University, Sendai 980-8578, Japan 2Department of Chemistry, Institute of Science Tokyo, Tokyo 152-8551, Japan 3Graduate School of Natural Science and Technology, Okayama University, Okayama 700-8530, Japan

(Received 12 June 2024; revised 1 April 2025; accepted 11 July 2025; published 4 September 2025)

Electronic ferroelectrics, with polarization P induced by strongly correlated charges, are expected to show ultrafast, huge, and flexible responses required in future optoelectronics. Although the challenges for ultrafast manipulation of such a polarization are ongoing, the expected advantages have been unclear. In this Letter, we demonstrate an unprecedentedly large increase by a factor of 2.7 in optical second harmonic generation at room temperature in the prototypical electronic ferroelectrics, the rare-earth ferrite LuFe<sub>2</sub>O<sub>4</sub>, by applying a terahertz field of 260 kV/cm. The transient anisotropy indicates that the direction of macroscopic polarization can be controlled three dimensionally on subpicosecond timescales, offering additional degrees of freedom in controlling polarization. Although the polarization response is in phase concerning the terahertz field, its sensitivity increased with delay, indicating that cooperative interactions among microscopic domains play an important role in the unprecedented response.

DOI: 10.1103/fryl-jjnj

Electronic ferroelectrics, which were discovered at the beginning of this century [1–3], 80 years after the first confirmation of ferroelectrics [4], are one of the fascinating candidate materials for the future high-speed communication and optoelectronics in terahertz frequency range. It is unique for the macroscopic dipole P triggered by strongly correlated charges [5–7], namely, charge ordering (CO) arising from mutual Coulomb repulsion. Like other quantum materials [8–10], electronic ferroelectrics are expected to show ultrafast and gigantic electronic responses for being disentangled from ionic displacement, causing energy waste and crystal fatigue seen in conventional ferroelectrics. In addition, this nature may enable flexible control of the polarization in sign and orientation to provide greater degrees of freedom [11]. The challenges of ultrafast manipulation of such a P have already been addressed in

Published by the American Physical Society under the terms of the Creative Commons Attribution 4.0 International license. Further distribution of this work must maintain attribution to the author(s) and the published article's title, journal citation, and DOI. organic crystals [3,12–18]. Still, the expected advantages of the sensitivity and/or flexibility have not been demonstrated, probably because of their inherent low dimensionality and lower electron density than transition metal oxides.

Layered iron oxides  $RFe_2O_4$  (R = Lu, Yb, Tm) [2,19] having the ferroelectric CO at room temperature [20] are promising for applications. As shown in Fig. 1, the crystal consists of doubled FeO layers (W layer) having a triangular lattice in the ab plane. While the average valence of Fe ions is 2.5+, three-dimensional CO sets in below the transition temperature  $T_{\rm CO} \approx 350 \, \text{K}$  accompanying the Fe<sup>2+</sup>/Fe<sup>3+</sup> superstructure in a layer with geometrically frustrated threefold periodicity (Fig. 2). The resultant charge imbalance between the neighboring layers forms the polar W layer. Thus, its stack, with RO2 layers in between, induces macroscopic polarization P lying in the ac plane (Fig. 1). Such a three-dimensional **P** without the constraint of lattice deformation may be anisotropically tailored to provide ultrafast functionality, exploiting a directional degree of freedom. For example, upon applying an electric field, P is expected to be tilted not only within the ac plane (upper right of Fig. 2) but also out of it (upper left), breaking the inherent symmetry.

Much studies have been performed on this CO and its electric field effect (~ kV/cm) [7,19] (in Supplemental Material [21], we briefly outlined the research history). Although some studies have cast doubt upon the scenario of the electronic ferroelectricity [22–30], the recent oxygen-stoichiometric high-quality single crystal has been

<sup>\*</sup>Contact author: hri@kwansei.ac.jp

<sup>&</sup>lt;sup>†</sup>Present address: Department of Physics and Astronomy, Kwansei Gakuin University, Sanda 669-1330, Japan.

<sup>&</sup>lt;sup>‡</sup>Present address: National Institutes for Quantum and Radiological Science and Technology, Sayo 679-5148, Japan.

Contact author: okimoto.y.aa@m.titech.ac.jp

Contact author: s-iwai@tohoku.ac.jp

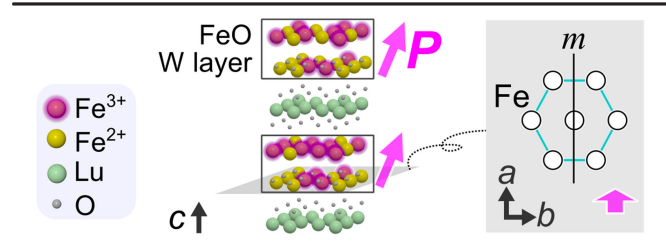


FIG. 1. Schematics of LuFe<sub>2</sub>O<sub>4</sub>. The Fe W layer (ab plane) and Lu-layer stacking along the c axis characterize the crystal structure. Polarization P arising from CO or Fe<sup>2+</sup>/Fe<sup>3+</sup> super-structure lies in the ac plane (mirror plane).

confirmed to show the CO having long-range coherence [31] via an optical second harmonic generation (SHG) experiment, accompanying a noncentrosymmetric monoclinic  $C_m$  point symmetry with P in the ac mirror plane (Fig. 1) (|P| was estimated as 12.9 C/cm² for YbFe<sub>2</sub>O<sub>4</sub>) [20]. The concomitant macroscopic responses have been exemplified by efficient terahertz wave generation [32], magnetoelectric effect [33], and dc-field-induced phase transition [34], giving prospects in interplay with the ultrafast dynamics of charges [35,36] or spins [37,38]. However, neither anisotropic control of P nor its noticeably large response have been confirmed.

Here we report the results of terahertz-pump SHG-probe spectroscopy of  $\text{LuFe}_2\text{O}_4$  (Fig. 2) at room temperature, revealing the sensitive and highly flexible nature of the electronic-ferroelectric polarization P. The SHG which directly reflects P [20] has been found to show, upon applying a 100 kV/cm-class terahertz electric field, the largest increase (by a factor of 2.7 at 260 kV/cm) among bulk ferroelectrics within a picosecond. The emergent anisotropy was successfully analyzed by a nonlinear susceptibility tensor with additional components reflecting terahertz-induced tilting of P.

The polar plots in Fig. 2 show SHG anisotropy, i.e., the dependence of the b- (left) and a-polarized (right) SHG intensity  $(I_{SH})$  on the polarization of the incident light (on the ab plane,  $\theta = 0^{\circ}$  represents the a axis). The SHG light was measured in reflection geometry (Supplemental Material Fig. S1 [21]) without the phase mismatch effect; the coherence length (~1.8 μm) is much longer than its penetration depth (≃100 nm) [21]. The blue closed circles reproduce the previously reported  $I_{SH}$  anisotropy at steady state (i.e., without the terahertz pump) [20]. With the electric field E of the incident fundamental light,  $(E_a, E_b) \equiv E_0(\cos \theta, \sin \theta)$ , and second-order nonlinear susceptibility d activated by P, nonlinear polarization  $P_i^{\rm NL} = \varepsilon_0 d_{ijk} E_j E_k$  is induced yielding  $I_{\rm SH||b} \propto (P_b^{\rm NL})^2 \propto$  $(d_{26}\sin\theta\cos\theta)^2$  accompanying the fourfold symmetry (blue line in the left panel), and  $I_{SH||a} \propto (d_{11} \sin^2 \theta +$  $d_{12}\cos^2\theta)^2$  (right) [21]. They do not show the signature of threefold P, which may coexist in the crystal with a triangular lattice.

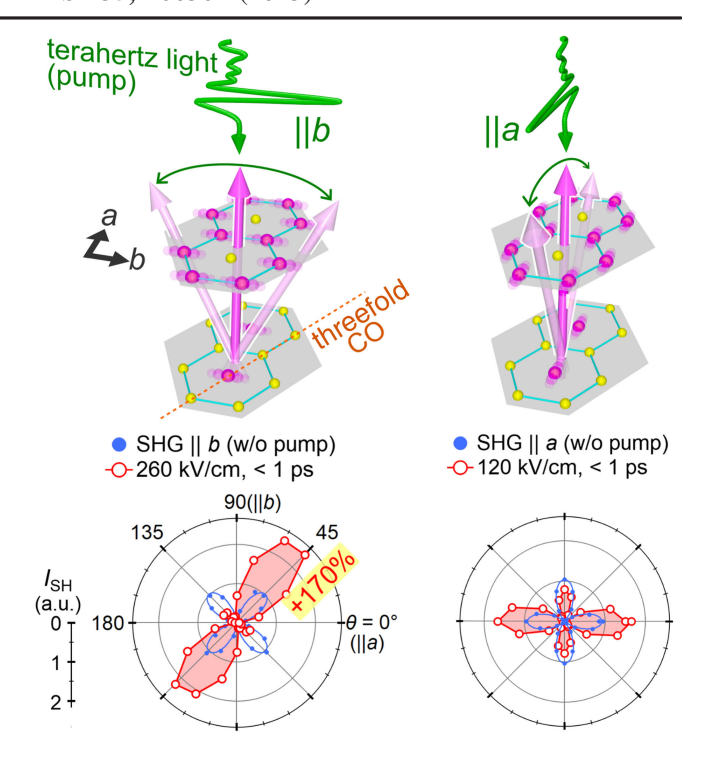


FIG. 2. Schematics of the terahertz-pump SHG-probe experiment. Terahertz electric field polarized along the b (left panel) and a axis (right panel) was introduced onto the single crystal, and the resultant P dynamics were probed by the b- and a-polarized SHG, respectively (Supplemental Material Fig. S1 [21] shows the experiment setup). Polar plots represent the dependences of SHG intensity on the polarization angle of the incident light ( $\theta = 0^{\circ}$  and  $90^{\circ}$  represents a and b axes, respectively). Anisotropies reflecting the steady-state P (blue) are significantly modulated to show an increase by a factor of 2.7 or +170% (red) instantaneously.

To manipulate P, the terahertz electric field  $E_{\mathrm{THz}}$  was introduced to modulate  $I_{\mathrm{SH}}$  as shown by the polar plots in Fig. 2 (red open circles). Remarkably, with  $E_{\mathrm{THz}}||b\>$  at 260 kV/cm (left), the peak  $I_{\text{SH}||b}$  at  $\theta = 45^{\circ}$  showed an instantaneous increase by a factor of 2.7 corresponding to +170\% in the ratio of the terahertz-induced change.  $\Delta I_{\rm SH}/I_{\rm SH}$ . On the other hand, another maximal at 135° (or 315°) decreased to less than half to completely break the inherent fourfold symmetry (the time evolution will be shown later). Such a symmetry change was also observed for  $E_{\text{THz}}||a|$  (right). These sensitive responses of LuFe<sub>2</sub>O<sub>4</sub> accompanying the emergent anisotropy should be the hallmark of the expected flexibility. The tensor analysis given later shows that the results for  $E_{\mathrm{THz}}||b|$  are characterized by the tilt of **P** breaking the ac mirror plane (upper left of Fig. 2).

Terahertz control of P in other bulk ferroelectrics is actively ongoing [13,15,16,39–49], taking advantage of its field strength which is much stronger than a typical coercive field (an electric field required to invert P) of conventional ferroelectrics [50], as well as its fixed carrier-

TABLE I. Preceding reports on terahertz-induced SHG increases of bulk ferroelectrics.  $\Delta I_{\rm SH}/I_{\rm SH}$  for LuFe<sub>2</sub>O<sub>4</sub> is +170% (i.e.,  $I_{\rm SH}$  increased by a factor of 2.7), while those for other bulk ferroelectrics are at most tens of percent, with 100 kV/cm-class  $E_{\rm THz}$ . LuFe<sub>2</sub>O<sub>4</sub> also marks a large value even at weak  $E_{\rm THz}$  (21% at 30 kV/cm), larger than those at comparable field strength. Note that with a far-stronger 16 MV/cm field Pb<sub>5</sub>(Ge, Si)<sub>3</sub>O<sub>11</sub> has marked a 3700% increase [39].

	$\Delta I_{ m SH}/I_{ m SH}$	$E_{\rm THz}~({\rm kV/cm})$
LuFe <sub>2</sub> O <sub>4</sub> (this Letter)	170%	260
	21%	30
Hdppz-Hca [40]	1.8%	250
BiCoO <sub>3</sub> [41]	12%	200
LiNbO <sub>3</sub> [42]	0.8%	100
$H_2C_2O_5$ [43]	20%	160
BiFeO <sub>3</sub> [44,53]	11%	210
$Pb_5(Ge, Si)_3O_{11}$ [39]	78%	280
$\alpha$ -(ET) <sub>2</sub> I <sub>3</sub> (10 K) [15]	2.6%	60
TTF-CA (90 K) [16]	2.9%	420

envelope phase [51,52] enabling coherent control. Notably, the SHG increase observed for LuFe<sub>2</sub>O<sub>4</sub> (170% at 260 kV/cm) is far more extensive than preceding reports; as summarized in Table I, they are at most tens of percent at 100 kV/cm-class fields [e.g., 0.8% for LiNbO<sub>3</sub> (100 kV/cm), 78% for Pb<sub>5</sub>(Ge, Si)<sub>3</sub>O<sub>11</sub> (280 kV/cm)]. The large  $\Delta I_{\rm SH}/I_{\rm SH}$  in LuFe<sub>2</sub>O<sub>4</sub> likely reflects the characteristic dynamics found in the terahertz range, as discussed later. It is expected to be even enhanced in the thin film form as seen in other ferroelectric devices [53].

To explore the terahertz-induced dynamics, we have measured the time evolution of  $I_{\rm SH||b}$  ( $I_{\rm SH}$  hereafter) as a function of the time delay t (Fig. 3). As shown in Fig. 3(a), the maximal  $I_{\rm SH}$  at  $\theta=45^{\circ}$  was found to follow  $E_{\rm THz}$ , i.e., show in-phase increases and decreases without delay, demonstrating terahertz modulation of P.  $I_{\rm SH}$  does not show noticeable decrease after applying  $E_{\rm THz}$  without the sign of the resultant electronic heating. We do not identify oscillatory components due to coherent phonons [13,15,47], consistent with its electronic origin disentangled from ionic displacement; the inset shows that the small tails at t>2 ps originate from the  $E_{\rm THz}$  waveform. At  $t\lesssim 1$  ps, on the other hand,  $E_{\rm THz}$  and  $I_{\rm SH}$  are not identical, as discussed later.

Figure 3(b) compares  $\theta = 45^{\circ}$  (purple circles) and 135° (yellow triangles) at an early stage. They were similar at t < 0 ps before  $E_{\text{THz}}$  was applied, reflecting the inherent fourfold symmetry, but nonetheless were largely and oppositely modulated by  $E_{\text{THz}}$ , ensuring the anisotropy change as shown by the polar plot in the left panel of Fig. 2. This is clearly seen in Fig. 3(c), wherein  $I_{\text{SH}}(\theta)$  at several t indicated by vertical broken lines are shown. While  $I_{\text{SH}}$  before  $t \simeq 0.4$  ps rather resembled the inherent fourfold symmetry, at  $t \simeq 0.7$  ps or the  $E_{\text{THz}}$  maximum it became highly anisotropic as in Fig. 2. In turn, it immediately flipped at  $t \simeq 1.1$  ps as  $E_{\text{THz}}$  inverted its sign, showing the feasibility of

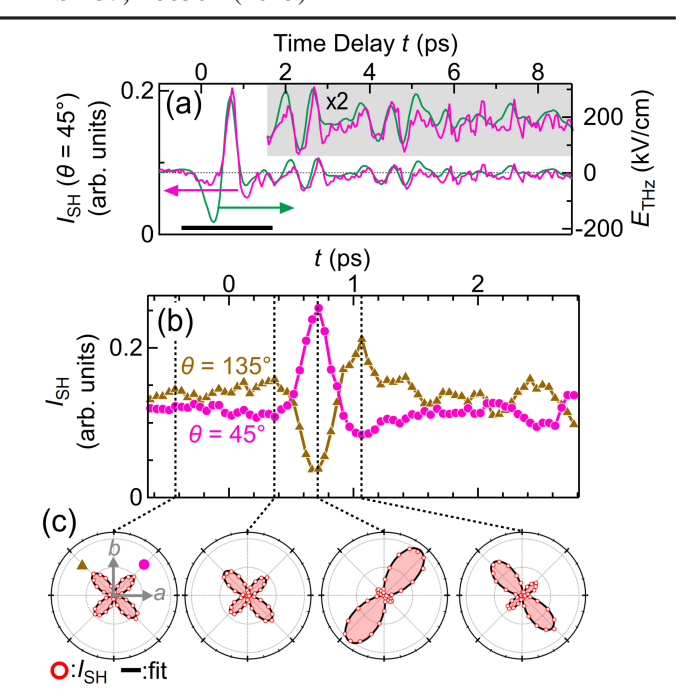


FIG. 3. Time evolutions of SHG (||b) anisotropy. (a)  $I_{\rm SH}$  observed with incident light polarization  $\theta=45^{\circ}$  and the  $E_{\rm THz}$  (||b) waveform applied to the LuFe<sub>2</sub>O<sub>4</sub> sample. (b)  $I_{\rm SH}(t)$  at  $\theta=45^{\circ}$  and 135° at an early stage. (c) Polar plots of  $I_{\rm SH}(\theta)$  at delays indicated by broken lines in (b). Solid lines show corresponding fitting curves.

coherent control. Supplemental Material Fig. S3 [21] shows time profiles for other components, including  $I_{SH||a}$ .

We analyzed the terahertz-induced anisotropy that the inherent  $C_m$  point group cannot explain. With the  $E_{\mathrm{THz}}||b$ , the ac mirror plane (Fig. 1) (the only symmetry operation) should be broken to give rise to the lowest symmetry P1. Corresponding tensor  $d^*$  is expressed as

$$d^* = \begin{pmatrix} d_{11}^* & d_{12}^* & d_{13}^* & d_{14}^* & d_{15}^* & d_{16}^* \\ d_{21}^* & d_{22}^* & d_{23}^* & d_{24}^* & d_{25}^* & d_{26}^* \\ d_{31}^* & d_{32}^* & d_{33}^* & d_{34}^* & d_{25}^* & d_{36}^* \end{pmatrix}, \tag{1}$$

yielding

$$I_{\text{SH}||b}(\theta) \propto \left(2d_{26}^* \sin \theta \cos \theta + d_{21}^* \cos^2 \theta + d_{22}^* \sin^2 \theta\right)^2$$
 (2)

with additional terms of  $d_{21}^*$  and  $d_{22}^*$  which were absent in the steady state. This formulation is validated by the much longer penetration depth of the used  $\approx 1$  terahertz light ( $\approx 100 \ \mu m$  [35]) than that of the SHG. We have also confirmed that the  $E_{\rm THz}$ -induced change of the fundamental light state or the phase matching condition, which may affect  $I_{\rm SH}$  [56], is negligibly small [21]. The fitting unambiguously converged [21], and the resultant curve [black lines in Fig. 3(c)] well reproduced the observed emergent anisotropy, indicating the absence of a

multidomain state with antiparallel P which may cause a failure of the fitting [21]. Here, the subpicosecond modulation of the anisotropy is analyzed as the transient change of  $d^*$  which is attributable to the dynamics of P from which  $d^*$  originates. The terahertz-induced modulation of SHG can also be interpreted in terms of third-order nonlinearity where electric fields of the fundamental and the terahertz light interact [54,55,57]; although the anisotropy may be analyzed using the inherent third-order susceptibility, it cannot explain the observed dynamics [21].

After all,  $d_{22}^*$ ,  $d_{21}^*$ , and  $d_{26}^*$  were successfully derived from each set of  $I_{\rm SH}(\theta)$  at various delay times t. The used  $E_{\rm THz}$  with peak value  $E_0 \equiv 240~{\rm kV/cm}$  is shown in Fig. 4(a); the attenuated  $E_{\rm THz}$  ( $E_0/2$ ,  $E_0/4$ , and  $E_0/8$ ) were also used. The results are summarized in Figs. 4(b)–4(d) after normalization by  $d_{26}$  being the only nonzero component in the steady state. Before  $E_{\rm THz}$  is applied ( $t < 0~{\rm ps}$ ),  $d^*$  are consistent with the steady state:  $d_{22}^* \simeq 0$ ,  $d_{21}^* \simeq 0$ , and  $d_{26}^* \simeq d_{26}$ .

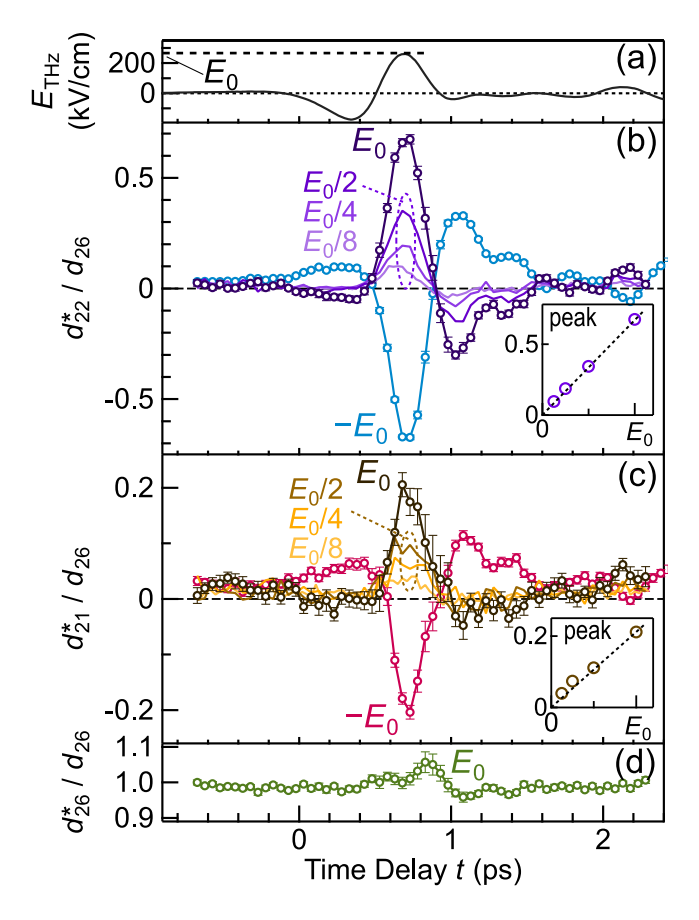


FIG. 4. Time evolutions of terahertz-induced nonlinear susceptibility tensor components  $d^*$ . (a) The  $E_{\rm THz}$  waveform with a maximum of 240 kV/cm ( $\equiv E_0$ ) applied to the LuFe<sub>2</sub>O<sub>4</sub> sample (||b). (b)–(d)  $d_{22}^*$ ,  $d_{21}^*$ , and  $d_{26}^*$  normalized by the steady-state value  $d_{26}$  derived from the fittings. Error bars, which are as small as marker circles, represent standard deviations of the fitting. For  $d_{22}^*$  and  $d_{21}^*$ , dependences on  $E_0$  are shown with insets showing peak values of  $d^*$ .

As Fig. 4(b) shows,  $d_{22}^*$  upon the strongest  $E_{\rm THz}$  (denoted as  $E_0$ ) first became nonzero ( $d_{22}^* < 0$ ) at  $t \simeq 0.3$  ps. It reached the maximum and minimum at around 0.7 and 1.0 ps, respectively, following the  $E_{\rm THz}$  waveform like  $I_{\rm SH}(t)$  at  $\theta=45^\circ$  [Fig. 3(b)]. The peak value is comparably large with the steady-state parameter ( $d_{22}^*/d_{26} \simeq 0.7$ ), underpinning the drastic symmetry change shown in the left panel of Figs. 2 and 3(c). This emergent  $d_{22}^*$  indicates that the polarization in the ac plane (Fig. 1) can be ultrafastly tilted out of it (upper left of Fig. 2), revealing the expected flexibility of the three-dimensional electronic ferroelectrics.  $d_{21}^*$  and  $d_{26}^*$  were smaller than  $d_{22}^*$  [Figs. 4(c) and 4(d)]; this might be related to the  $E_{\rm THz}$  polarization [21].

The time evolutions of  $d_{22}^*$  are similar among the used  $E_{\rm THz}$  from  $E_0/8$  to  $E_0$ , and the peak value linearly increased with  $E_{\rm THz}$  [inset of Fig. 4(b)]. Accordingly, the inverted  $E_{\rm THz}$  ( $-E_0$ ) triggered the similar dynamics except for the sign of  $d^*$ ; in this sense,  $E_{\rm THz}||\pm b|$  are equivalent, consistent with the ac mirror plane.

As shown in Figs. 4(a) and 4(b), the emergent component  $d_{22}^*(t)$  (at  $E_0$ , for example) has its minima and maxima at the same times as those for  $E_{\rm THz}(t)$  without retardation, similar to  $I_{\rm SH}(t)$  [Fig. 3(a)]. It should be noted, however, that their time profiles are not identical. For  $d_{22}^*$  at  $E_0$ , the second minimum ( $\approx$ 1.0 ps) is deeper than the first one ( $\approx$ 0.3 ps) despite the shallower second peak for  $E_{\rm THz}$ ; the equivalent occurs at  $-E_0$ , i.e., irrespective of the  $E_{\rm THz}$  polarity. This indicates that  $d^*$  becomes more sensitive around 1.0 ps than around 0.3 ps. Such a behavior differs from previous reports on other compounds [13,15,40,43,44,54,57] where the time profile of polarization follows the  $E_{\rm THz}$  waveform [21].

Figure 5(a) shows  $d_{22}^*$  (circles) and corresponding  $E_{\rm THz}$  (dotted line) normalized at their peaks around 0.7 ps. To

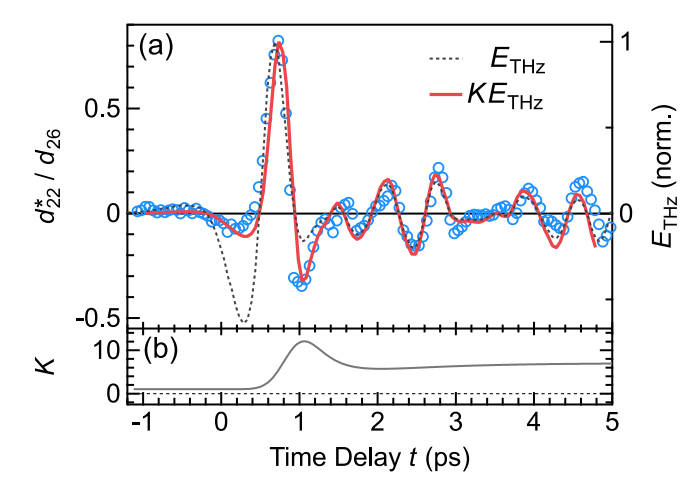


FIG. 5. Incubation time of  $d_{22}^*$ . (a)  $d_{22}^*/d_{26}$  and normalized  $E_{THz}$  waveform. K in the fitting curve  $K(t)E_{THz}$  represents an assumed coefficient corresponding to the sensitivity of  $d^*$ . (b) The sensitivity introduced in Eq. (3).

reproduce the discrepancy at  $t \lesssim 1$  ps, we assumed a linear coefficient K(t) as the sensitivity of  $d^*$  based on the linear response of  $d^*$  to  $E_{\text{THz}}$  [inset of Fig. 4(b)]. As shown, the curve  $KE_{\text{THz}}$  (red line) agrees well with  $d_{22}^*$ . The used K shown in Fig. 5(b) has an exponential rise and a decay component,

$$K = (\Theta(t^*) [A_r \{ 1 - e^{-\tau_r/t^*} \} + A_d e^{-\tau_d/t^*}] + 1) * G, \quad (3)$$

with time constants of  $\tau_r=1$  ps and  $\tau_d=0.3$  ps, respectively, convoluted with a 0.45 ps FWHM Gaussian function G. Here,  $\Theta$  is a step function,  $t^*\equiv t-0.86$  ps,  $A_r=6$ , and  $A_d=10$ . While K=1 at t<0 ps, it peaks at  $t\simeq 1$  ps to become an order of magnitude larger, followed by the residue surviving for several picoseconds. The dynamic rise in the  $d_{22}^*$  sensitivity indicates that the response of P is accompanied by a delay or accumulation effect. In other words, the observed anomalous time profile cannot be reproduced by a mere nonlinearity against  $E_{\text{THz}}$ .

It is notable that such a delayed response, referred to as incubation time, has been also observed in other systems as a result of photoinduced phase transitions accompanying a cooperative effect [10]. The difference in microscopic mechanisms is reflected in timescales during the process: tens of seconds for spin-lattice interaction in spin-crossover systems [58,59], picoseconds for strain wave in a Mott insulator [60]. The characteristic subpicosecond delay observed for electronic ferroelectrics is therefore attributable to electronic or quantum-mechanical interactions among microscopic polarizations. Correspondingly, a sign of lattice contribution or coherent phonons is absent [Fig. 3 (a)]. While the individual electronic polarization is expected to show ultrafast (< 1 fs reflecting an energy scale of the Coulomb repulsion) response following  $E_{THz}$  at an early stage, it takes ≈1 ps for them to cooperatively interact and proliferate to become more macroscopic, accompanying the considerable sensitivity. Furthermore, it is inferred from the incubation time that the energy scale of the interaction between the microscopic polarizations is on the order of a few meV.

The scenario is supported by the preceding optical-pump experiment [36]; the photoinduced transient enhancement of P(||c) was identified within a picosecond and attributed to the growth of interlayer charge coherence. The  $E_{\rm THz}$  in this study may act as a similar stimulus to effectively increase P or the concomitant K [Fig. 5(b)]. It is also plausibly interpreted as a kind of field-induced ferroelectricity [47]; the nonpolar domains, which are accidentally formed by errors in charge arrangement, may be rearranged by the  $E_{\rm THz}$  to become polar enhancing the net P.  $E_{\rm THz}$  -induced formation of a new charge pattern could be another possibility for the enhancement.

We speculate that the threefold CO (Fig. 2) or the charge fluctuations due to the geometrical frustration plays an essential role in this unique process and/or the large  $I_{\rm SH}$ 

increase. Relatively higher density of electrons in LuFe<sub>2</sub>O<sub>4</sub> might also be responsible, as compared to molecular-based electronic ferroelectrics with smaller  $\Delta I_{\rm SH}/I_{\rm SH}$  [1.2 × 10<sup>22</sup> cm<sup>-3</sup> for LuFe<sub>2</sub>O<sub>4</sub> while, for example, 0.6 × 10<sup>21</sup> cm<sup>-3</sup> for  $\alpha$ -(ET)<sub>2</sub>I<sub>3</sub>].

In summary, we demonstrate an unprecedentedly large 170% increase of SHG at room temperature in LuFe $_2$ O $_4$  by applying a terahertz electric field of 260~kV/cm. The transient nonlinear optical susceptibilities indicate that macroscopic polarization direction can be controlled on subpicosecond timescales. The increase in polarization sensitivity is delayed, indicating that cooperative interactions between the microscopic domains play an essential role in the large response.

Acknowledgments—The authors thank A. Ono, M. Naka, and H. Adachi for fruitful discussions. This work was supported by JST CREST (Grant No. JPMJCR1901), MEXT Q-LEAP (Grant No. JPMXS0118067426), JSPS KAKENHI (Grants No. JP15H02100, No. JP17K14317, No. JP18H01144, No. JP18H05208, No. JP20K03800, No. JP20H05147, No. JP22H01149, and No. JP23K22420), Hattori Hokokai Foundation, and Toyota Riken Scholar.

- [1] P. Monceau, F. Y. Nad, and S. Brazovskii, Phys. Rev. Lett. 86, 4080 (2001).
- [2] N. Ikeda, H. Ohsumi, K. Ohwada, K. Ishii, T. Inami, K. Kakurai, Y. Murakami, K. Yoshii, S. Mori, Y. Horibe, and H. Kitô, Nature (London) 436, 1136 (2005).
- [3] K. Yamamoto, S. Iwai, S. Boyko, A. Kashiwazaki, F. Hiramatsu, C. Okabe, N. Nishi, and K. Yakushi, J. Phys. Soc. Jpn. 77, 074709 (2008).
- [4] J. Valasek, Phys. Rev. 17, 475 (1921).
- [5] T. Portengen, T. Östreich, and L. J. Sham, Phys. Rev. B 54, 17452 (1996).
- [6] J. van den Brink and D. I. Khomskii, J. Phys. Condens. Matter **20**, 434217 (2008).
- [7] S. Ishihara, J. Phys. Soc. Jpn. 79, 011010 (2010).
- [8] D. N. Basov, R. D. Averitt, and D. Hsieh, Nat. Mater. 16, 1077 (2017).
- [9] A. De la Torre, D. M. Kennes, M. Claassen, S. Gerber, J. W. McIver, and M. A. Sentef, Rev. Mod. Phys. 93, 041002 (2021).
- [10] S. Koshihara, T. Ishikawa, Y. Okimoto, K. Onda, R. Fukaya, M. Hada, Y. Hayashi, S. Ishihara, and T. Luty, Phys. Rep. 942, 1 (2022).
- [11] G. Catalan, A. Lubk, A. H. G. Vlooswijk, E. Snoeck, C. Magen, A. Janssens, G. Rispens, G. Rijnders, D. H. A. Blank, and B. Noheda, Nat. Mater. 10, 963 (2011).
- [12] E. Collet, M.-H. Lemée-Cailleau, M. B.-L. Cointe, H. Cailleau, M. Wulff, T. Luty, S.-Y. Koshihara, M. Meyer, L. Toupet, P. Rabiller, and S. Techert, Science 300, 612 (2003).
- [13] T. Miyamoto, H. Yada, H. Yamakawa, and H. Okamoto, Nat. Commun. **4**, 2586 (2013).

- [14] H. Itoh, K. Itoh, K. Goto, K. Yamamoto, K. Yakushi, and S. Iwai, Appl. Phys. Lett. 104, 173302 (2014).
- [15] H. Yamakawa, T. Miyamoto, T. Morimoto, H. Yada, Y. Kinoshita, M. Sotome, N. Kida, K. Yamamoto, K. Iwano, Y. Matsumoto, S. Watanabe, Y. Shimoi, M. Suda, H. M. Yamamoto, H. Mori, and H. Okamoto, Sci. Rep. 6, 20571 (2016).
- [16] T. Morimoto, T. Miyamoto, H. Yamakawa, T. Terashige, T. Ono, N. Kida, and H. Okamoto, Phys. Rev. Lett. 118, 107602 (2017).
- [17] H. Itoh, R. Fujiwara, Y. Kawakami, K. Yamamoto, Y. Nakamura, H. Kishida, and S. Iwai, Appl. Phys. Lett. 112, 093302 (2018).
- [18] H. Itoh, H. Obatake, R. Fujiwara, Y. Kawakami, K. Yamamoto, M. Dressel, and S. Iwai, Phys. Rev. Res. 3, L032043 (2021).
- [19] N. Ikeda, T. Nagata, J. Kano, and S. Mori, J. Phys. Condens. Matter 27, 053201 (2015).
- [20] K. Fujiwara, Y. Fukada, Y. Okuda, R. Seimiya, N. Ikeda, K. Yokoyama, H. Yu, S. Koshihara, and Y. Okimoto, Sci. Rep. 11, 4277 (2021).
- [21] See Supplemental Material at http://link.aps.org/supplemental/10.1103/fryl-jjnj for (1) an overview of research on RFe<sub>2</sub>O<sub>4</sub>, (2) the experiment setup, (3) SHG anisotropy and conversion efficiency in the steady state, (4) terahertz-induced dynamics of SHG anisotropy, (5) terahertz-induced effects on the fundamental frequency pulse, (6) fitting analysis of the SHG anisotropy, (7) on the possibility of a multidomain state, (8) analysis based on third-order nonlinear susceptibility, and (9) transient sensitivity.
- [22] M. Angst, R.P. Hermann, A.D. Christianson, M.D. Lumsden, C. Lee, M.-H. Whangbo, J.-W. Kim, P.J. Ryan, S.E. Nagler, W. Tian, R. Jin, B.C. Sales, and D. Mandrus, Phys. Rev. Lett. 101, 227601 (2008).
- [23] M. Angst, Phys. Status Solidi RRL 7, 383 (2013).
- [24] A. Ruff, S. Krohns, F. Schrettle, V. Tsurkan, P. Lunkenheimer, and A. Loidl, Eur. Phys. J. B 85, 290 (2012).
- [25] D. Niermann, F. Waschkowski, J. de Groot, M. Angst, and J. Hemberger, Phys. Rev. Lett. 109, 016405 (2012).
- [26] J. de Groot, T. Mueller, R. A. Rosenberg, D. J. Keavney, Z. Islam, J.-W. Kim, and M. Angst, Phys. Rev. Lett. 108, 187601 (2012).
- [27] J. Bourgeois, M. Hervieu, M. Poienar, A. M. Abakumov, E. Elkaïm, M. T. Sougrati, F. Porcher, F. Damay, J. Rouquette, G. Van Tendeloo, A. Maignan, J. Haines, and C. Martin, Phys. Rev. B 85, 064102 (2012).
- [28] A. J. Hearmon, D. Prabhakaran, H. Nowell, F. Fabrizi, M. J. Gutmann, and P. G. Radaelli, Phys. Rev. B 85, 014115 (2012).
- [29] X. S. Xu, J. de Groot, Q.-C. Sun, B. C. Sales, D. Mandrus, M. Angst, A. P. Litvinchuk, and J. L. Musfeldt, Phys. Rev. B 82, 014304 (2010).
- [30] A. Glamazda, K.-Y. Choi, P. Lemmens, D. Wulferding, S. Park, and S.-W. Cheong, Phys. Rev. B 87, 144416 (2013).
- [31] K. Fujiwara, T. Karasudani, K. Kakurai, W. T. Lee, K. C. Rule, A. J. Studer, and N. Ikeda, J. Phys. Soc. Jpn. 88, 044701 (2019).
- [32] H. Yu, Y. Okimoto, A. Morita, S. Shimanuki, K. Takubo, T. Ishikawa, S. Koshihara, R. Minakami, H. Itoh, S. Iwai, N.

- Ikeda, T. Sakagami, M. Nozaki, and T. Fujii, Materials 16, 1989 (2023).
- [33] Y. Fukada and N. Ikeda, J. Phys. Soc. Jpn. **90**, 113705 (2021).
- [34] S. Konishi, D. Urushihara, T. Hayakawa, K. Fukuda, T. Asaka, K. Ishii, N. Naoda, M. Okada, H. Akamatsu, H. Hojo, M. Azuma, and K. Tanaka, Phys. Rev. B 108, 014105 (2023).
- [35] H. Itoh, K. Itoh, K. Anjyo, H. Nakaya, H. Akahama, D. Ohishi, S. Saito, T. Kambe, S. Ishihara, N. Ikeda, and S. Iwai, J. Lumin. 133, 149 (2013).
- [36] H. Yu, Y. Fukada, G. Nishida, K. Takubo, T. Ishikawa, S. Koshihara, N. Ikeda, and Y. Okimoto, Phys. Rev. Mater. 8, 064402 (2024).
- [37] J. Lee, S. A. Trugman, C. D. Batista, C. L. Zhang, D. Talbayev, X. S. Xu, S.-W. Cheong, D. A. Yarotski, A. J. Taylor, and R. P. Prasankumar, Sci. Rep. 3, 2654 (2013).
- [38] J. Lee, S. A. Trugman, C. L. Zhang, D. Talbayev, X. S. Xu, S.-W. Cheong, D. A. Yarotski, A. J. Taylor, and R. P. Prasankumar, Appl. Phys. Lett. 107, 042906 (2015).
- [39] V. Bilyk, E. Mishina, N. Sherstyuk, A. Bush, A. Ovchinnikov, and M. Agranat, Phys. Status Solidi RRL 15, 2000460 (2021).
- [40] T. Umanodan, K. Kaneshima, K. Takeuchi, N. Ishii, J. Itatani, H. Hirori, Y. Sanari, K. Tanaka, Y. Kanemitsu, T. Ishikawa, S. Koshihara, S. Horiuchi, and Y. Okimoto, J. Phys. Soc. Jpn. 88, 013705 (2019).
- [41] Y. Okimoto, S. Naruse, R. Fukaya, T. Ishikawa, S. Koshihara, K. Oka, M. Azuma, K. Tanaka, and H. Hirori, Phys. Rev. Appl. 7, 064016 (2017).
- [42] A. von Hoegen, R. Mankowsky, M. Fechner, M. Först, and A. Cavalleri, Nature (London) 555, 79 (2018).
- [43] T. Miyamoto, D. Hata, T. Morimoto, H. Yamakawa, N. Kida, T. Terashige, K. Iwano, H. Kishida, S. Horiuchi, and H. Okamoto, Sci. Rep. 8, 15014 (2018).
- [44] N. Sono, Y. Kinoshita, N. Kida, T. Ito, H. Okamoto, and T. Miyamoto, J. Phys. Soc. Jpn. 90, 033703 (2021).
- [45] I. Katayama, H. Aoki, J. Takeda, H. Shimosato, M. Ashida, R. Kinjo, I. Kawayama, M. Tonouchi, M. Nagai, and K. Tanaka, Phys. Rev. Lett. 108, 097401 (2012).
- [46] F. Chen et al., Phys. Rev. B 94, 180104(R) (2016).
- [47] X. Li, T. Qiu, J. Zhang, E. Baldini, J. Lu, A. M. Rappe, and K. A. Nelson, Science 364, 1079 (2019).
- [48] K. Asada, T. Miyamoto, H. Yamakawa, J. Hirata, N. Takamura, T. Morimoto, K. Suzuki, T. Otaki, N. Kida, T. Nakamura, and H. Okamoto, Phys. Rev. B 104, 195148 (2021).
- [49] Y. Okimoto, P. Xia, J. Itatani, H. Matsushima, T. Ishikawa, S. Koshihara, and S. Horiuchi, APL Mater. 10, 090702 (2022).
- [50] J. F. Scott, Science 315, 954 (2007).
- [51] T. Kampfrath, K. Tanaka, and K. A. Nelson, Nat. Photonics **7**, 680 (2013).
- [52] J. A. Fülöp, S. Tzortzakis, and T. Kampfrath, Adv. Opt. Mater. 8, 1900681 (2020).
- [53] There are also studies of films. A BiFeO<sub>3</sub> film showed an 8% increase at 0.4 MV/cm [54], while a ferroelectric-paraelectric-composite Sm-BiFeO<sub>3</sub> device with field-enhancing slit-structured electrodes marked ~220× increase

- [54]. A  $Ba_{0.8}Sr_{0.2}TiO_3$  film showed ~140× increase at 1 MV/cm [55].
- [54] F. Chen, J. Goodfellow, S. Liu, I. Grinberg, M. C. Hoffmann, A. R. Damodaran, Y. Zhu, P. Zalden, X. Zhang, I. Takeuchi, A. M. Rappe, L. W. Martin, H. Wen, and A. M. Lindenberg, Adv. Mater. 27, 6371 (2015).
- [55] K. Grishunin, V. Bilyk, N. Sherstyuk, V. Mukhortov, A. Ovchinnikov, O. Chefonov, M. Agranat, E. Mishina, and A. V. Kimel, Sci. Rep. 9, 697 (2019).
- [56] M. Cornet, J. Degert, E. Abraham, and E. Freysz, Opt. Lett. 39, 5921 (2014).
- [57] K. A. Grishunin, N. A. Ilyin, N. E. Sherstyuk, E. D. Mishina, A. Kimel, V. M. Mukhortov, A. V. Ovchinnikov, O. V. Chefonov, and M. B. Agranat, Sci. Rep. 7, 687 (2017).
- [58] Y. Ogawa, S. Koshihara, K. Koshino, T. Ogawa, C. Urano, and H. Takagi, Phys. Rev. Lett. **84**, 3181 (2000).
- [59] H. Watanabe, H. Hirori, G. Molnár, A. Bousseksou, and K. Tanaka, Phys. Rev. B 79, 180405(R) (2009).
- [60] T. Amano et al., Nat. Phys. 20, 1778 (2024).